Photonic Nambu-Goldstone bosons

Miguel-Ángel García-March,[1] Angel Paredes,[2], Mario Zacarés,[3] Humberto Michinel[2] and Albert Ferrando,[4]
[1] *ICFO – Institut de Ciències Fotòniques, The Barcelona Institute of Science and Technology, 08860 Castelldefels (Barcelona), Spain.*
[2] *Área de Òptica, Departamento de Física Aplicada, Universidade de Vigo, As Lagoas s/n, Ourense, ES-32004 Spain.*
[3] *Facultad de Veterinaria y Ciencias Experimentales, Universidad Católica de Valencia, 'San Vicente Martir", (València), Spain.*
[4] *Departament d'Òptica i Optometria i Ciències de la Visió. Interdisciplinary Modeling Group, InterTech. Universitat de València, Burjassot (València), Spain.*

We predict the existence of a Nambu-Goldstone excitation in the propagation of light in nonlinear periodic lattices. We use methods of condensed matter physics that emphasize the peculiarities stemming from the interplay between the nonlinearity and the lattice periodicity. By means of *nonlinear* Bloch and Wannier functions we provide an explicit construction of the effective free energy of the system, valid for long-range, or, equivalently, low-energy excitations around Bloch solutions. Using then Landau mean field theory for phase transitions we determine the possible stable ground states of the optical system and their stability conditions. Low energy excitations above a stable ground state are fully controlled by the $U(1)$ phase of the optical field, which appear as a Nambu-Goldstone boson, analogous to those predicted in condenser matter and particle physics systems. We support these results by numerical simulations both for spatially periodic and finite nonlinear Bloch wave solutions. We demonstrate how finite-sized nonlinear Bloch light structures embedded in a linear periodic lattice act as tunable metawaveguides for the phase Nambu-Goldstone waves.

I. INTRODUCTION

Nonlinearities have played a key role in discovering an amazing wealth of phenomena in laser beam propagation, in the manipulation of light and in establishing connections between optics and other areas of physics. Many analogies with condensed matter physics have been presented in the literature, see e.g. [1–3]. Optical versions have appeared for different kinds of spatially ordered lattices as, e.g., honeycomb graphene-like configurations [4] or Lieb lattices [5]. Remarkable concepts like the topological protection of transport properties have been translated from the condensed matter community to photonic systems [6–8]. In most situations, the underlying photonic structure is a linear or nonlinear refractive index which satisfies certain periodicity conditions along the plane transverse to beam propagation. It naturally induces an ordering in the distribution of light which can be (partially) identified with the wavefunction of electrons within crystals. It has been recently shown that the spatial ordering can also arise spontaneously for appropriately chosen nonlocal nonlinearities [9].

In this context, the present work deals with pattern formation and light propagation in nonlinear lattices [10, 11]. We consider square lattices, a symmetry that has been studied in relation to guiding of light [12], formation of discrete solitons [13], supercontinuum generation [14], lasers [15] and metamaterials [16], just to mention a few examples. Our goal is to introduce methods that are customarily used in the solid state literature [17] but that have not been fully exploited in the framework of nonlinear optics. We provide a simple effective description that is an approximation to the full dynamics of the system. This is done by first integrating out the dynamics inside each lattice cell in order to write down a discrete model. Then, we go back to the continuum by considering excitations of long wavelength compared to the lattice spacing, giving rise to a mean field formulation. The microscopic details of the underlying system get encoded in the values of a number of coefficients for the effective free energy. This procedure is, in spirit, analogous to renormalization in condensed matter or particle physics.

The effective description for an order parameter allows us to discuss the stability of the stationary solutions and their lowest lying excitations. We emphasize that the nonlinearity is an essential ingredient for our procedure. The introduced formalism can shed new light on results directly obtained from the complete model and is instrumental in formulating new predictions. In this work, we focus on one of them: the existence of a perturbation of the phase that can be interpreted as a Nambu-Goldstone boson. We also show how finite size propagating nonlinear beams inside a photonic lattice can act as effective "metawaveguides" for these Nambu-Goldstone phase waves, as depicted in Fig. 1. Remarkably, the propagation properties of the phase wave depend on the nature of the underlying nonlinear beam, which in this way behaves as an optical "metamaterial" with tunable susceptibilities.

It is well known that the nonlinear Schrödinger equation on which our work is grounded is also the mean-field description of Bose-Einstein condensates [18]. Thus, our results can also find application in the semiclassical modeling of cold atoms in optical lattices [19].

The paper is organized as follows: in Section II we in-

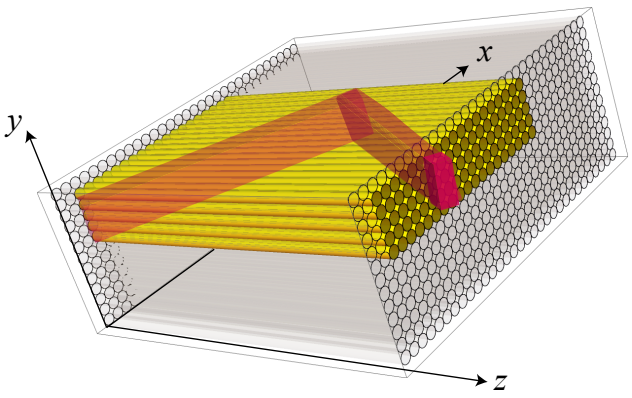

FIG. 1: A finite size nonlinear solution (yellow structure) with adequate features propagating inside a photonic lattice acts as an effective metawaveguide for phase excitations of the optical field (red path). These phase waves behave as photonic Nambu-Goldstone bosons.

troduce the mathematical model and comment on its relation to nonlinear propagation in photonic lattices. We also define the nonlinear Wannier functions that will be used in the following sections. In Section III, we introduce the concept of free energy into our model and its effective description, based on a series of approximations. In Section IV we use the condensed matter formalism to analyze the nature of the ground state and its relation to the stability of different solutions contrasting these results with full-fledged numerical computations. In Section V, we characterize a phase perturbation and show that it can be identified with the Nambu-Goldstone boson coming from spontaneous symmetry breaking of global phase shifts. In Section VI, we analyze finite size solutions that lead us to the concept of metawaveguide for phase waves. Finally, in Section VII we conclude and outline possible future directions. In Appendix A, we introduce in a rather detailed and pedagogical way the concepts of Bloch and Wannier functions, for readers that might not be familiar with the formalism. Appendix B gives a precise definition of what we define as the phase at each lattice cell.

II. THE MODEL

In order to model paraxial nonlinear propagation of monochromatic light, we consider the dimensionless nonlinear Schrödinger equation in the following form

$$i\frac{\partial\psi}{\partial z} = -\nabla^2\psi + V(x,y)\psi - g|\psi|^2\psi, \tag{1}$$

where $g = +1$ or $g = -1$, depending on the focusing or defocusing character of the Kerr nonlinearity and ∇^2 is the two-dimensional Laplacian. The potential of the linear term is assumed to be periodic, defining cells of unit size which form a square lattice,

$$V(x,y) = V(x+1,y) = V(x,y+1). \tag{2}$$

For definiteness, computations will be performed using

$$V = V_0\cos^2(\pi x)\cos^2(\pi y). \tag{3}$$

We choose this particular potential because of its simplicity and because it can be generated by illuminating a photorefractive material with a standard interference pattern [20]. Equation (1) and therefore most of our discussion can be applied to the dynamics of Bose-Einstein condensed cold atoms. In that context, Eq. (3) is a typical profile for two-dimensional optical lattices [21] although it is well-known that other potentials are also possible [22].

The discussion and general conclusions of this work depend decisively on Eq. (2) but not on the concrete expression Eq. (3). The nonlinear refractive index can also be space-dependent as long as it respects the symmetry of Eq. (2). A simple alternative to Eq. (3) would be to consider inclusions of regions with a certain refractive index in a bulk with different properties, resulting in a piecewise constant V. This can be accomplished with laser-written waveguides [23, 24] or in typical photonic crystal fibers [25–27]. An interesting possibility is that of hollow core fibers since the linear and nonlinear properties can be tuned by appropriately filling them with a gas [28, 29].

As a convenient mathematical trick, customarily used in condensed matter physics, we also introduce periodic boundary conditions for the wavefunction

$$\psi(x,y) = \psi(x+N,y) = \psi(x,y+N), \tag{4}$$

for some integer $N \gg 1$, such that there are N^2 unit cells in the lattice. Obviously, the condition of Eq. (4) is unphysical. We will relax it in Section VI, where finite structures are considered. Most of the features found using Eq. (4) apply to realistic setups.

The Hamiltonian density can be defined as

$$\mathcal{H} = \nabla\psi^*\cdot\nabla\psi + V(x,y)|\psi|^2 - \frac{1}{2}g|\psi|^4. \tag{5}$$

We define its integral as the energy and notice that the norm of the wavefunction is related to the power of the optical beam:

$$E = \int \mathcal{H}dxdy, \qquad P = \int |\psi|^2 dxdy. \tag{6}$$

It is straightforward to check from Eq. (1) that $dP/dz = dE/dz = 0$.

A stationary solution of Eq. (1) takes the form $\psi = e^{-i\mu z}\varphi(x,y)$ for a real propagation constant μ with

$$\mu\varphi = -\nabla^2\varphi + V(\mathbf{x})\varphi - g|\varphi|^2\varphi. \tag{7}$$

In the following, we compute the dynamical evolution of the wavefunction by numerically integrating Eq. (1)

with a standard beam propagation method. Stationary solutions of Eq. (7) can be computed with the same method by propagating in imaginary time.

This dimensionless formalism is connected to photonic propagation in a periodic medium as follows. The standard paraxial wave equation for a laser beam reads

$$-2ik_0n_0\frac{\partial A}{\partial \tilde{z}} = \tilde{\nabla}^2 A + 2\Delta n k_0^2 n_0 A, \tag{8}$$

where $k_0 = \omega/c = 2\pi/\lambda$ is the wavenumber in vacuum and A is the wave envelope, slowly varying at the scale of the wavelength. Dimensionful spatial coordinates are denoted as $\tilde{x}$, $\tilde{y}$, $\tilde{z}$ and the laplacian is $\tilde{\nabla}^2 \equiv \partial_{\tilde{x}}^2 + \partial_{\tilde{y}}^2$. The refractive index is $n = n_0 + \Delta n$ where n_0 is a constant and for $\Delta n \ll n_0$ we consider the sum of a nonlinear component and a linear part associated to the inhomogeneity of the optical material $\Delta n = \frac{n_2 n_0}{2\eta_0}|A|^2 + \Delta n_{lin}(\tilde{x},\tilde{y})$, where n_2 is the nonlinear refractive index and $\eta_0 = \sqrt{\mu_0/\epsilon_0}$. We now assume that $\Delta n_{lin}(\tilde{x},\tilde{y})$ is periodic in space, $\Delta n_{lin}(\tilde{x},\tilde{y}) = \Delta n_{lin}(\tilde{x}+a,\tilde{y}) = \Delta n_{lin}(\tilde{x},\tilde{y}+a)$ where a is the lattice spacing. We can rescale Eq. (8) in order to bring it to dimensionless form, Eq. (1), by taking

$$\begin{aligned} (\tilde{x},\tilde{y}) &= a(x,y)\ , \quad A = \frac{1}{n_0 k_0 a}\sqrt{\frac{\eta_0}{|n_2|}}\psi, \\ \tilde{z} &= 2k_0 n_0 a^2 z\ , \qquad \Delta n_{lin} = -\frac{1}{2n_0 k_0^2 a^2}V. \end{aligned} \tag{9}$$

In particular, notice that V scales with a^2 and therefore the value of V_0 can be tuned by adjusting the lattice spacing. For instance, imagine a sample value of $n_0 = 1.5$, and a maximum deviation of the linear refractive index $|\Delta n_{lin}| = 0.1$. Then, the value $V_0 = 800$ that will be used in sections III-VI for the illustratory examples corresponds to $a \approx 8\lambda$. The relation between the dimensionless power and the physical one is

$$\tilde{P} = \frac{\lambda^2}{8\pi^2 n_0 |n_2|}P. \tag{10}$$

As it is somewhat customary [30–32], we will abuse language and identify the propagation distance $\tilde{z}$ with a "time" parameterizing the evolution. From this point of view, we refer to the velocity of a perturbation $\tilde{v}$ (which is an angle in physical terms) as the displacement in $\tilde{x}$, $\tilde{y}$ divided by $\tilde{z}$. The relation to the dimensionaless velocity is

$$\tilde{v} = \frac{\lambda}{4\pi n_0 a}v. \tag{11}$$

In the linear case ($g = 0$), the structure of the lowest-lying stationary solutions of Eqs. (1), (2), (4) with the translationally invariant potential, Eq. (3), are readily obtained by means of Bloch and Wannier functions [33]. We describe these functions in detail in appendix A for the reader who is not acquainted with this formalism. Here we first discuss the nonlinear Bloch functions and we highlight their differences with respect to the linear ones. Consider a stationary configuration

$$\psi = e^{-i\mu_{\mathbf{Q}} z}\varphi^P_{\mathbf{Q}}(\mathbf{x}), \tag{12}$$

which solves the stationary Eq. (7). Here $\varphi^P_{\mathbf{Q}}(\mathbf{x})$ has the form of Eq. (A1) and therefore is labelled by its pseudomomentum $\mathbf{Q}$ [with N^2 discretized possible values given in Eq. (A4)]. One important difference with respect to the linear case is that they are obtained by solving Eq. (A5) self-consistenly, that is taking the potential for this equation as

$$V_{sol} = V(\mathbf{x}) - g|\varphi^P_{\mathbf{Q}}(\mathbf{x})|^2. \tag{13}$$

Notice that V_{sol} satisfies the same periodicity conditions (2) and therefore the nonlinear Bloch functions can be defined for it following the procedure of Appendix A. The nonlinear Bloch functions have appeared already in the literature in various contexts [34–39]. We consider here only the N^2 nonlinear Bloch waves of the lowest band. Then in Eq. (12) the only indexes for φ are the pseudomomentum $\mathbf{Q}$ and P. The introduction of this last index is a crucial difference with the linear case: the solution depends on the power. Notice that, since the propagation constant $\mu_{\mathbf{Q}}(P)$ depends on the power, the nonlinear Bloch functions depend on μ.

An important goal of the present work is to study the stability and perturbations of these solutions (see Section III). With that purpose, we compute, following the procedure of appendix A, the N^2 Bloch functions associated to the potential of Eq. (13), that we denote $\varphi^{P,sol}_{\mathbf{Q}}(\mathbf{x})$, and introduce the corresponding nonlinear Wannier functions,

$$W^P_{\mathbf{R}}(\mathbf{x}) = \frac{1}{N\sqrt{P}}\sum_{\mathbf{Q}} e^{-i\mathbf{Q}\cdot\mathbf{R}}\varphi^{P,sol}_{\mathbf{Q}}(\mathbf{x}), \tag{14}$$

where the sum runs over the N^2 Bloch momenta and $\mathbf{R}$ takes values corresponding to the center of the N^2 lattice sites [see Eq. (A7)]. Note that they also depend on P. By construction, $\varphi^P_{\mathbf{Q}}(\mathbf{x})$ is itself a Bloch function of the V_{sol} potential and therefore, according to Eq. (A9), it can be written as

$$\varphi^P_{\mathbf{Q}}(\mathbf{x}) = \sum_{\mathbf{R}} c_{\mathbf{R}} W^P_{\mathbf{R}}(\mathbf{x}), \quad \text{with} \quad c_{\mathbf{R}} = \frac{\sqrt{P}}{N}e^{i\mathbf{R}\cdot\mathbf{Q}}. \tag{15}$$

The most convenient basis is the one defined for the nonlinear problem at hand, taking into account the solution to be perturbed. The Wannier functions $W^P_{\mathbf{R}}(\mathbf{x})$ are crucial in the effective theory presented in the next section, which, as a first application, allows us to study the stability of the nonlinear Bloch solutions.

III. EFFECTIVE DESCRIPTION FOR THE FREE ENERGY

The goal of this section is to introduce a simple effective theory that allows us to understand and predict

general features of the propagation of light described by the model of Eq. (1). We will do it by borrowing definitions and methods from condensed matter theory. We will then verify the conclusions by comparing them to direct numerical computations.

We start by introducing the optical equivalent of the free energy

$$F = E - \mu P. \tag{16}$$

In terms of statistical physics, P plays the role of the number of particles and μ corresponds to the chemical potential. Along a family of stationary nonlinear solutions, we find the relations $\mu = \partial E/\partial P$ and $P = -\partial F/\partial \mu$, linked by the Legendre transform (16). In this way, the known relation for a family of nonlinear solutions $P = P(\mu)$ or its inverse $\mu = \mu(P)$, can be understood as the equation of state in the equivalent system. This can be proved by considering a perturbation $\mu \to \mu + \delta\mu$, $\varphi(\mathbf{x}) \to \varphi(\mathbf{x}) + \delta\varphi(\mathbf{x})$. Keeping only the leading terms in the perturbation, we can write $\delta P = \int (\varphi^* \delta\varphi + \text{ c.c.}) d^2\mathbf{x}$ and $\delta E = \int (\delta\varphi[-\nabla^2\varphi^* + V\varphi^* - g|\varphi|^2\varphi^*] + \text{ c.c.}) d^2\mathbf{x}$, where c.c. stands for complex conjugate. Using Eq. (7), it is straightforward to check that $\delta E = \mu \delta P$. The variation of the free energy within the family of solutions is given by $\delta F = \delta E - \mu\delta P - P\delta\mu = -P\delta\mu$.

The free energy (16) can be expressed as an integral over the entire domain Ω

$$F = \int_\Omega d^2\mathbf{x} \left(\nabla\varphi^* \nabla\varphi + V(\mathbf{x})|\varphi|^2 - \frac{g}{2}|\varphi|^4 - \mu|\varphi|^2 \right). \tag{17}$$

Integrating by parts and using Eq. (7), we find that its value for a stationary solution is

$$F = \frac{g}{2} \int_\Omega d^2\mathbf{x} |\varphi|^4, \tag{18}$$

and therefore it is just characterized by the nonlinear interaction.

The next step is to integrate out the dynamics at each cell of the lattice in order to produce a discrete model. With this goal, we use the expansion (15) in terms of nonlinear Wannier functions to rewrite the free energy (17) in terms of the N^2 coefficients $c_\mathbf{R}$ associated to each cell. For simplicity, we restrict ourselves to solutions with

$$Q_x = Q_y = \frac{2\pi m}{N} \equiv q, \quad m \in \left(-\frac{N}{2} + 1, \ldots, \frac{N}{2} \right), \tag{19}$$

which present $x \leftrightarrow y$ symmetry. Then, keeping only the on-site and nearest neighbor integrals of the Wannier functions, we find

$$F = \sum_\mathbf{R} \left(-t(\mu) \sum_{\nu=1}^{4} c^*_\mathbf{R} c_{\mathbf{R}+\mathbf{n}_\nu} + l(\mu)|c_\mathbf{R}|^2 - \frac{U(\mu)}{2}|c_\mathbf{R}|^4 \right) + \sum_\mathbf{R} \left(-I(\mu)|c_\mathbf{R}|^2 \sum_{\nu=1}^{4} (c^*_\mathbf{R} c_{\mathbf{R}+\mathbf{n}_\nu} + c^*_{\mathbf{R}+\mathbf{n}_\nu} c_\mathbf{R}) \right) + \ldots \tag{20}$$

where the $\mathbf{n}_\nu$ are the vectors connecting nearest neighbors, (1,0), (0,1), (-1,0), (0,-1) and the dots represent higher order terms. We have introduced the real quantities

$$\begin{aligned} t(\mu) &= -\int_\Omega W^{P*}_\mathbf{R} \left(-\nabla^2 + V(\mathbf{x}) - \mu \right) W^P_{\mathbf{R}+\mathbf{n}_1} d^2\mathbf{x}, \\ l(\mu) &= \int_\Omega W^{P*}_\mathbf{R} \left(-\nabla^2 + V(\mathbf{x}) - \mu \right) W^P_\mathbf{R} d^2\mathbf{x}, \\ U(\mu) &= g \int_\Omega |W^P_\mathbf{R}|^4 d^2\mathbf{x}, \\ I(\mu) &= g \int_\Omega |W^P_\mathbf{R}|^2 W^{P*}_\mathbf{R} W^P_{\mathbf{R}+\mathbf{n}_1} d^2\mathbf{x}, \end{aligned} \tag{21}$$

which are independent of the site $\mathbf{R}$ because of the translational symmetry of the Wannier functions. In this expression, we have made explicit that t, l, U and I depend on the power P and —due to the the equation of state $\mu = \mu(P)$— on the propagation constant μ, because they are computed from the corresponding nonlinear Wannier functions, see Sec. II. In Fig. 2, we represent the values of these coefficients found numerically for a few examples.

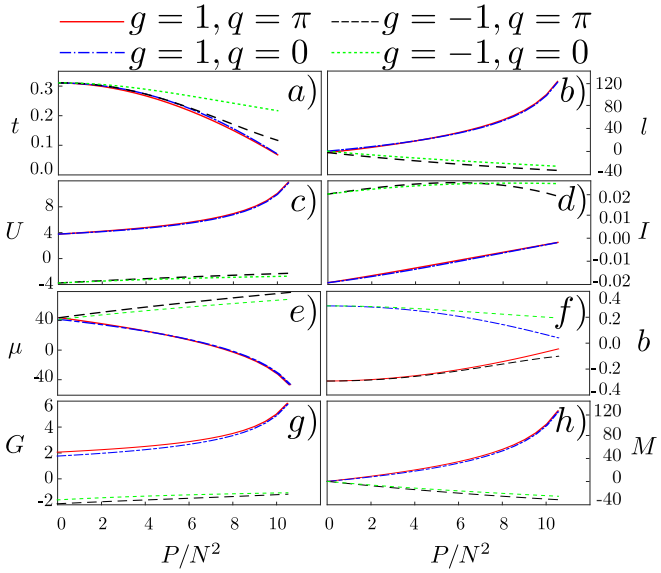

FIG. 2: In panels a)-d), the values of the integrals of Eqs. (21) are shown for four cases with different nonlinearity and different $\mathbf{Q}$, with fixed $V_0 = 800$, $N = 24$. Additionally, the low energy coefficients appearing in Eqs. (23) and (25), for the effective free energy, and in the field potential (26) are shown in panels e)-h) in terms of the normalized power P/N^2. In all cases —except in the remarkable case f)— the blue and red lines are practically overlapping and in the plot are seen as a single solid line corresponding to $g = 1$ with $q = 0$ and $q = \pi$, respectively. On the contrary, figure f) unveils that the sign of b is positive for $q = 0$ and negative for $q = \pi$.

In the language of the discretized theory, small perturbations around the stationary solution of Eq. (15) are described by promoting the $c_\mathbf{R}$ to z-dependent functions, in

such a way the uniform amplitude of the nonlinear Bloch function is substituted by a slowly varying $\mathbf{R}$-dependent envelope function

$$c_{\mathbf{R}}(z) = \Phi_{\mathbf{R}}(z) e^{i\mathbf{R}\cdot\mathbf{Q}}. \tag{22}$$

The theory can be further simplified by going to a new description in the continuum, valid for perturbations $\delta\Phi_{\mathbf{R}}$ with a typical length scale $\delta\mathbf{R}$ larger than the lattice spacing a. This is accomplished by transforming the summation over the $\mathbf{R}$ lattice sites of Eq. (20) into an integral, with $\Phi_{\mathbf{R}}(z) \to \Phi(\mathbf{x}, z)$. We write the resulting free energy as

$$\begin{aligned} F &= \int_\Omega d^2\mathbf{x} \Bigg[b\nabla\Phi^*\nabla\Phi + \left(M|\Phi|^2 - \frac{\mathcal{G}}{2}|\Phi|^4 \right) + \\ &+ I(\cos q)\Big(4|\Phi|^2|\nabla\Phi|^2 + \Phi^{*2}(\nabla\Phi)^2 + \Phi^2(\nabla\Phi^*)^2 \Big) + \\ &- 2i(\sin q)(t + 2I|\Phi|^2)\Phi^*(\partial_x\Phi + \partial_y\Phi) \Bigg], \end{aligned} \tag{23}$$

with

$$b = t\cos q, \quad \mathcal{G} = \frac{U}{2} + 8I\,\cos q, \quad M = l - 4t\cos q. \tag{24}$$

IV. LANDAU THEORY, SPONTANEOUS SYMMETRY BREAKING AND STABILITY

The expression of Eq. (23) is the sought effective description of the system that allows us to determine the stability of stationary solutions and to study the nature of the ground state. In view of Eqs. (15) and (22), the solutions with a definite pseudomomentum $\mathbf{Q}$ of the form ($A1$) correspond in the effective description to a continuous field with a uniform envelope $\Phi = \Phi_0$.

In order to simplify the discussion, we deal with the leading order terms in $I(\mu)$ (compare in Fig. (2) the scale for $I(\mu)$ in panel d) to the rest of quantities) and, for reasons that will be clear next, neglect the last anisotropic term in Eq.(23). We then define the effective free energy describing the ground state and their low energy excitations as

$$\begin{aligned} \bar{F} &= \mathrm{sgn}(b) F = \int_\Omega d^2\mathbf{x} \Bigg[|b| \nabla\Phi^*\nabla\Phi \\ &+ \mathrm{sgn}(b) \left(M|\Phi|^2 - \frac{\mathcal{G}}{2}|\Phi|^4 \right) + \dots \Bigg]. \end{aligned} \tag{25}$$

This change of sign does not alter the dynamics but ensures a positive kinetic term, as it is essential to define a proper ground, or vacuum, state [40]. In this way, in a many-body description of the theory the lower energy pseudoparticles would correspond always to quanta owning positive kinetic energy no matter the sign of b. This feature guarantees that the vacuum (defined as the state with no particles) is indeed the state with lowest energy.

We now apply Landau theory, a mean-field approach used to characterize phase transitions in condensed matter and particle physics [41]. We have to verify whether a constant configuration $\Phi = \Phi_0 \neq 0$ can minimize (25). For $\sin q \neq 0$, that is not possible because long wavelength perturbations, e.g. $\Phi_0 \exp(ikx)$, produce a smaller $\bar{F}$ due to the anisotropic last term in Eq.(23) (this fact justifies the absence of the anisotropic term in Eq.(25)). Therefore, we must set $q = 0$, i.e., $\mathbf{Q} = (0, 0)$ (see panel (a) of Fig. 12) or $q = \pi$, i.e., $\mathbf{Q} = (\pi, \pi)$ (panel (d) of Fig. 12). We refer to these configurations as unstaggered and staggered, respectively, borrowing the condensed matter terminology for ferromagnetic and antiferromagnetic spin systems.

From Eq. (25) we see that, due to the fact that the kinetic term is now positive definite, a $\Phi = \Phi_0$ minimum of $\bar{F}$ exists if and only if it is a minimum of the effective field potential term

$$V(\Phi) = \mathrm{sgn}(b) \left(M|\Phi|^2 - \frac{\mathcal{G}}{2}|\Phi|^4 \right). \tag{26}$$

It is immediate to check that the nontrivial minimum condition $\Phi = \Phi_0 \neq 0$ is achieved when $(b\ M) < 0$ and $(b\ \mathcal{G} < 0)$. The plots of Fig. 2 show that this happens for the cases $g = 1$, $q = \pi$ and $g = -1$, $q = 0$. This is clearly visualized in Fig. 3.

Thus, we find that for attractive nonlinearity, the ground state stable configuration is the staggered one whereas for repulsive nonlinearity it is the unstaggered one. The form of V in Eq. (3) is not crucial for this result, which holds for generic types of periodic potentials. Heuristically, one may think of this result as a minimization of the on-shell free energy (18), assuming that $|\varphi|^2$ is more spread out in the unstaggered configuration, leading to a smaller $\int |\varphi|^4 d^2\mathbf{x}$ and that the opposite happens for the staggered solution (cf. Fig. 11).

In addition, the effective potential for a typical stable configuration, as shown in Fig. 3, presents the paradigmatic Mexican hat shape. This potential is characteristic of the spontaneous symmetry breaking mechanism appearing in condensed matter, like in superfluids or superconductors [42], and particle physics systems, like in the Higgs mechanism [43]. In situations described by this type of potential, the ground state is degenerate (white circle of radius $|\Phi_0|$ in Fig. 3) presenting a continuous phase degeneracy: $\Phi_0(\alpha) = |\Phi_0| e^{i\alpha}$. Despite the original free energy (25) and equation of motion are invariant under $U(1)$ phase transformations, the ground state $\Phi_0(\alpha)$ is not since it changes under a phase shift $\Phi_0(\alpha) \neq \Phi_0(\alpha + \theta)$. This fact has profound implications in the nature of the low energy spectrum of excitations, as we will see in the next section.

In this approach, the stability of the ground state is equivalent to the stability of the original nonlinear Bloch solution, represented by the uniform envelope Φ_0 at a fixed value of P/N^2. Note that, oppositely, when $g = 1$, $q = 0$ or $g = -1$, $q = \pi$, the effective potential is inverted $V(\Phi) \to -V(\Phi)$, so that the uniform solution

$\Phi = \Phi_0 \neq 0$ is then a maximum of the free energy and, thus, becomes unstable. This fact implies that the original nonlinear Bloch solutions (15) are unstable for the unstaggered (staggered) configuration in the case of attractive (repulsive) nonlinearity.

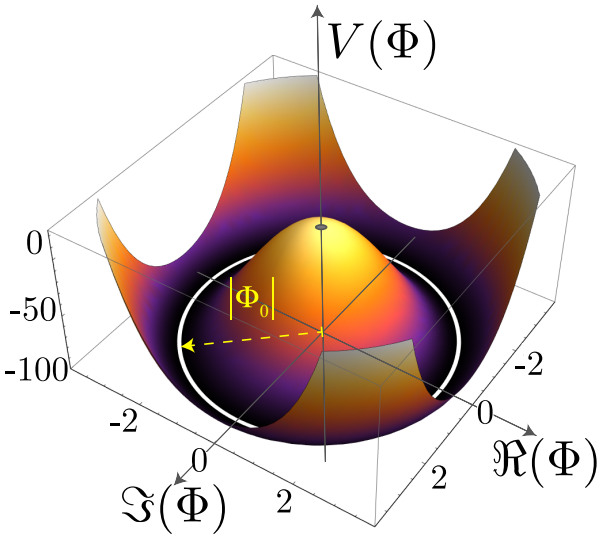

FIG. 3: *Calculated* effective field potential $V(\Phi)$ for a self-focusing ($g = 1$) and staggered ($q = \pi$) solution in a lattice with fixed $V_0 = 800$ and $N = 24$ as in Fig. 2. The power per site is $P/N^2 = 2$ so that $b = -0.3$, $M = 11$ and $\mathcal{G} = 2.2$. The same Mexican hat shape is obtained in all cases (for these values of V_0 and N) provided $g = 1$ and $q = \pi$ or $g = -1$ and $q = 0$.

In Fig. 4, these conclusions are confronted with direct numerical integration of Eq. (1). We depict the result of the evolution of three different initial stationary solutions, with focusing nonlinearity. As expected from the discussion above, the only one that remains stable upon propagation is the staggered one. For the other two, the initial phase pattern eventually breaks down and the distribution of power becomes inhomogeneous among the different cells. We have also verified that for the case of defocusing nonlinearity $g = -1$, only the unstaggered solution is stable.

Some configurations, as for instance the $\mathbf{Q} = (\pi/2, \pi/2)$ one, can remain stable for large values of z. For those cases, the simplest way to check that $\mathbf{Q} = (\pi, \pi)$ is the real ground state is to introduce some random noise in the initial condition. What we see is that, for small values of z, the noise in the phase is apparent in the regions where $|\psi|^2$ is small but the phase remains ordered otherwise. Under evolution, the initial phase pattern breaks down, except for the staggered stable case.

Even if the computations have been spelled out for a particular example, we remark that the conclusion is rather robust, being applicable to large regions of the space of parameters. There are some limitations, on which we briefly comment now. In the small V_0 limit,

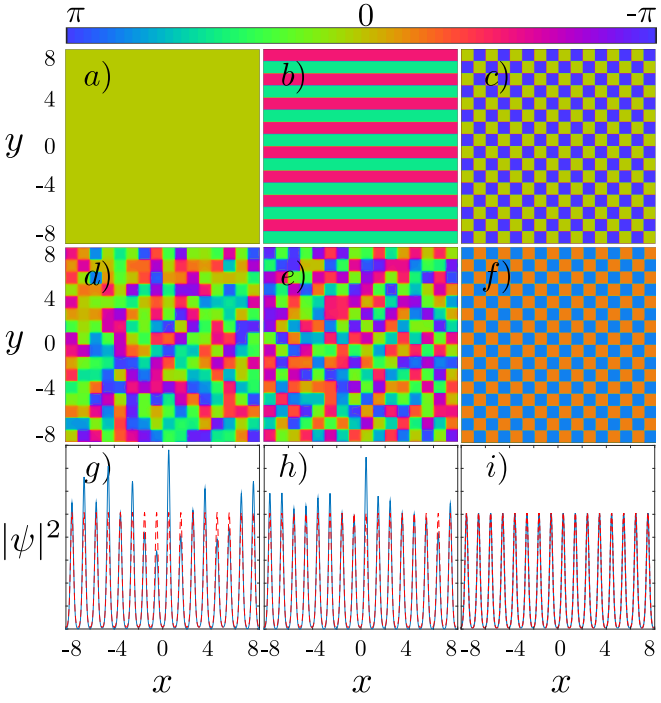

FIG. 4: Evolution, computed by numerical integration of Eq. (1), of three different stationary solutions with $g = 1$, $V_0 = 800$, $N = 16$, $P/N^2 = 5$. The unstaggered $\mathbf{Q} = (0, 0)$ is represented in panels a) (phase distribution at $z = 0$), d) (phase distribution at $z = 10$) and g) (the blue solid line represents a one-dimensional cut $|\psi(x, \frac{1}{2})|^2(z = 10)$ compared to the initial wavefunction depicted by the red dashed line $|\psi(x, \frac{1}{2})|^2(z = 0)$). With the same specifications, $\mathbf{Q} = (0, \pi)$ is represented in panels b), e), h) and $\mathbf{Q} = (\pi, \pi)$ in panels c), f), i). The figure shows that the staggered configuration $\mathbf{Q} = (\pi, \pi)$ is the only stable one.

our approximations break down since the lattice structure becomes irrelevant and therefore the discussion loses its validity. The same happens for large P, since, the wavefunction can self-focus and collapse in each cell (for $g = 1$) or overcome the periodic potential V due to self-repulsion (for $g = -1$). Moreover, since this is a nonlinear phenomenon in nature, cases with $P/N^2 \to 0$ have to be taken with care. This discussion based on Landau theory and on the effective description of Eq. (23) provides a new point of view for the interpretation of previous theoretical [44, 45] and experimental [46–48] results.

Going back to the effective description given by (25) and (26), the minimization of the effective potential V —and thus $\bar{F}$— requires

$$|\Phi_0|^2 = \frac{M}{\mathcal{G}}. \tag{27}$$

This quantity should be identified with the power in each lattice site. As a nontrivial crosscheck of the approximate effective model, we have verified that the value of $M/\mathcal{G}$ computed from Eqs. (21), (24) typically coincides with P/N^2 up to a deviation of a few percent.

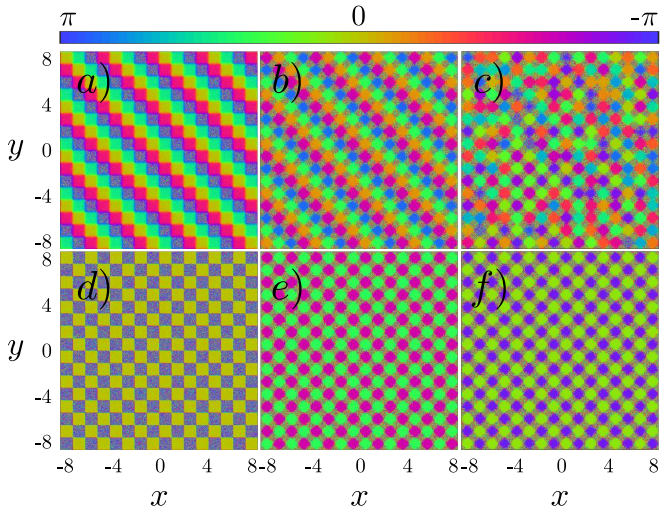

FIG. 5: Evolution of the phase for initial conditions with noise, fixing $g = 1$, $V_0 = 800$, $N = 16$, $P/N^2 = 5$. Panels a), b) and c) correspond to the $\mathbf{Q} = (\pi/2, \pi/2)$ case for $z = 0$, $z = 0.1$ and $z = 4$ respectively. Panels d), e) and f) correspond to $\mathbf{Q} = (\pi, \pi)$ for the same values of z. The noise is introduced by multiplying the initial phase at each point by a random number from a normal distribution of amplitude 0.2. It is visible that the phase structure gets destabilized in the $\mathbf{Q} = (\pi/2, \pi/2)$ case whereas it remains stable in the staggered configuration.

Finally, it is worth emphasizing that the dependence on μ —and, therefore, on P/N^2— of the coefficients of the effective theory, which paves the way for the analysis à la Landau, is the result of using the nonlinear Wannier functions in the modeling.

V. PHASE EXCITATIONS AS NAMBU-GOLDSTONE BOSONS

The effective description of Sec. III immediately yields another important dynamical observation. As mentioned previously, we have a typical case of spontaneous breaking of a continuous symmetry. Namely, $|\Phi_0|e^{i\alpha}$ in Eq. (27) minimizes the free energy for any $\alpha \in [0, 2\pi)$. The theory (23) is invariant under a $U(1)$ phase rotation, but its ground state is not. According to the well-known Goldstone's theorem [43], such a symmetry breaking is accompanied by the existence of a massless Nambu-Goldstone boson related to the motion in field space along the generators of the broken symmetry — in our case of the $U(1)$ phase symmetry. This perturbation is always the one dominating the low energy dynamics [49, 50], since it is easily excited, when compared to other degrees of freedom. Well known examples of Nambu-Goldstone bosons are phonons in superfluids or solids, magnons in ferromagnets [51] or the pions stemming from spontaneous chiral symmetry breaking in quantum chromodynamics [50]. Other closely related phenomena are the symmetry breaking leading to superconductivity or the Higgs boson. Thus, on general grounds, we expect to find long-range perturbations of the phase which propagate as waves throughout the domain, that can be identified with Nambu-Goldstone bosons. The goal of this section is twofold: on the one hand, we will show their existence by direct numerical computations and we will study their propagation, and, on the other hand, we will analytically prove how the effective free energy (25) indeed predicts the existence of massless phase excitations at low energies.

In order to illustrate the process, we take a stable stationary solution and introduce a phase shift in some of the lattice cells, see Fig. 6. In the example, we take a staggered solution with focusing nonlinearity and, at $z = 0$, we multiply the ψ of the cells of the central column by $e^{i\pi/5}$. We then integrate numerically Eq. (1) and depict how the perturbation of the phase propagates within the lattice, generating a wave moving leftwards and another one moving rightwards. We defer to appendix B a precise definition of the phase perturbation plotted in the figure. The modulus of ψ and, with it, the power per lattice cell, also gets perturbed. However, the size of its perturbation decreases as the P/N^2 of the background solution increases and is subdominant with respect to the phase oscillation. In this sense, we refer to the excitation as a perturbation of the phase and identify it with a Nambu-Golstone boson.

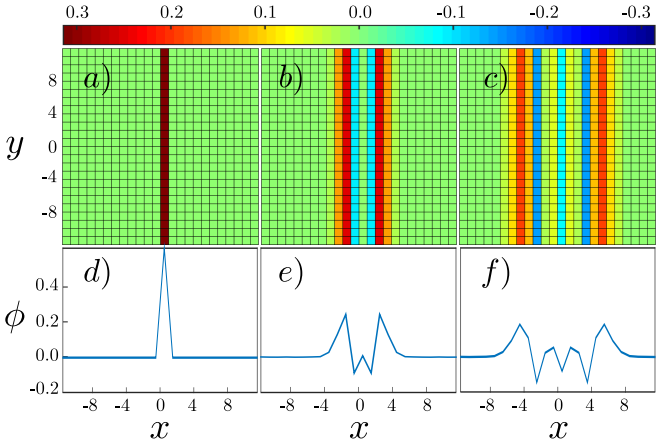

FIG. 6: Illustration of the propagation of the excitation of the phase ($g = 1$, $V_0 = 800$, $N = 24$, $P/N^2 = 5$). The initial condition is like that of panel c) of Fig. 4, multiplying by $e^{i\pi/5}$ the wavefunction for a column of lattice sites. Panels a)-c) depict the phase distribution for three values of z. Panels d)-f) are $y = 0$ cuts of the same quantity. Notice that in panel a) the strength of the perturbation ($\pi/5$) is higher than the maximum of the colormap scale, a convention chosen to improve visualization in panels b) and c).

From a simulation like the one of Fig. 6, we can infer the velocity of the wave by, e.g., following the position of the first peak moving leftwards and fitting its position in terms of z to a line. For fixed g and V_0, we find that

it does depend very mildly on the strength of the perturbation and on N. On the other hand, it does change significantly with the value of P/N^2 of the background solution, stressing the importance of the nonlinear effects and of the usage of the nonlinear Wannier functions.

We now discuss this dynamics in the framework of the effective model of Sec. III. Introducing a small perturbation

$$\Phi = \Phi_0(1+\gamma(\mathbf{x},z))\exp(i\alpha(\mathbf{x},z)) \quad (\gamma,\alpha\in\mathbb{R}) \qquad (28)$$

in the equation of motion $i\partial\Phi/\partial z = \delta\mathcal{F}/\delta\Phi^* - \nabla(\delta\mathcal{F}/\delta\nabla\Phi^*)$, where $\mathcal{F}$ is the integrand in Eq. (23) and assuming $\sin q = 0$, we find

$$\begin{aligned}\partial_z\gamma &= -\cos q(t+2I\Phi_0^2)\nabla^2\alpha,\\ \partial_z\alpha &= 2M\gamma - \cos q(t+6I\Phi_0^2)\nabla^2\gamma.\end{aligned} \qquad (29)$$

By taking the axial derivative in the second equation, substituting the value of $\partial_z\gamma$ according to the first equation and keeping only the leading order terms in the derivative expansion, one finds the equation fulfilled by the phase excitation α at long distances or, equivalently, at low energies:

$$\nabla^2\alpha - \frac{1}{v^2}\partial_z^2\alpha = 0. \qquad (30)$$

This equation is the wave equation in two spatial and one time dimensions (where z plays the role of the temporal coordinate). In the language of condensed matter and particle physics, this equation corresponds to the massless excitation associated to the phase, which is the Nambu-Goldstone boson associated to the symmetry broken by the ground state, namely, the $U(1)$ phase symmetry as depicted in the Mexican hat potential in Fig. 3. In addition, our calculation predicts an explicit expression for the phase velocity of the Nambu-Goldstone phase excitation:

$$v = \sqrt{-2M(\cos q)(t+2I|\Phi_0|^2)}. \qquad (31)$$

For the focusing unstaggered and defocusing staggered cases, which we found to be unstable in Sec. III, this v is imaginary, providing a new evidence of instability. For the focusing staggered and defocusing unstaggered cases, Eq. (31) gives an estimate that can be compared with the results of direct numerical integration of Eq. (1). This is done in Fig. 7. It is important to remark that M, t, I and $|\Phi_0|$ are all nontrivial functions of P^2/N, as shown in Fig. 2.

The wave equation (30) leads to a linear dispersion relation between ω —the conjugate variable of the evolution variable (t or z)— and the spatial wavevector $\mathbf{k}$: $\omega\sim|\mathbf{k}|$. This is a remarkable fact since the dispersion relation associated to the original free energy (25) for the envelope field Φ is quadratic: $\omega\sim|\mathbf{k}|^2$. In terms of spatio-temporal symmetries, the Galilean invariance of the original description in terms of a generalized nonlinear Schrödinger equation turns into the Lorentzian inviariance of the wave equation (30) for the α phase field. This is a known effect in condensed matter physics associated to the spontaneous breaking of phase symmetry, as in superfluidity and superconductivity [42, 49, 51]. A complete analysis in the language of effective field theories [50], but in terms of spontaneous symmetry breaking in non-relativistic systems provides the same answer [52–54].

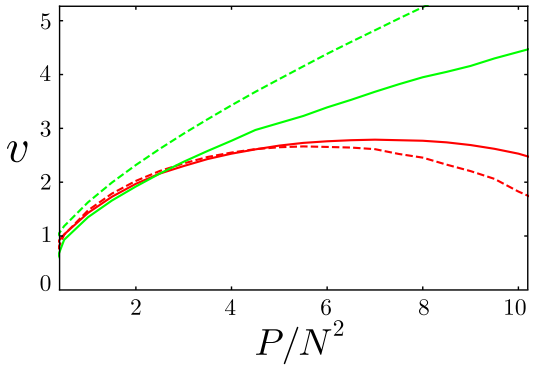

FIG. 7: Comparison of the wave velocity obtained from repeated numerical integration (solid line) of Eq. (1) and the one predicted by the effective model (dashed line) in Eq.(31) as a function of the power per lattice cell. The green upper curves correspond to the defocusing unstaggered case and the red lower curves correspond to the focusing staggered case. Notice that the horizontal axis starts at $P/N^2 = 0.5$ because when this quantity tends to zero the excitation loses its Nambu-Goldstone boson character.

The plot of Fig. 7 shows that the effective model correctly captures the qualitative features of the Nambu-Goldstone boson phase excitation. For small P/N^2, the velocity grows in an approximately linear fashion. This can be understood heuristically by noticing that, in the first term of Eq. (25), if we split Φ in modulus and phase, the kinetic term for the phase is multiplied by $\Phi_0^2 \approx P/N^2$. If we integrate in z to obtain the action, dz is multiplied by P/N^2, resulting in the mentioned linear dependence. For focusing nonlinearity, the velocity reaches a maximum and then decreases. This happens because the light distribution within each site gets more and more spatially confined, reducing the interaction with the neighboring sites. For larger values of P, the wavefunction would self-focus and collapse within each site (we notice that in the present dimensionless convention the critical power of the Townes profile is 11.7). One can also appreciate that the quantitative match of the model with the numerics is better in the focusing case. The interpretation is that for defocusing nonlinearity, the light distribution is more spread out and the notion of lattice discretization becomes less clear, limiting the quantitative validity of the approximation leading to Eq. (20) and thus to all expressions derived from it, including the one for v. Finally, let us remark that, as it happens in typical cases of particle or condensed matter physics, the quantitative precision of the approximation

could get better if additional terms are included in the expansion leading to the effective theory [50, 52, 53].

Of course, the profile of the wave depends on the symmetry of the initial conditions. In Fig. 8, we plot the result of initially perturbing the phase of four adjacent cells, resulting in a circular-shaped wave.

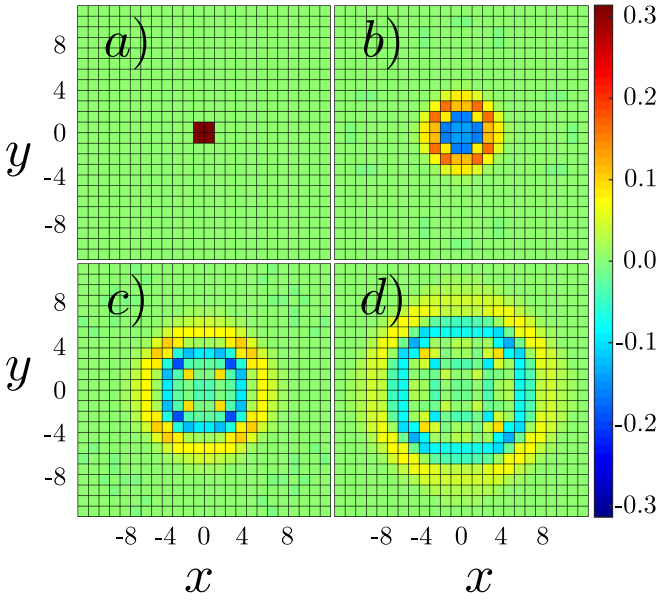

FIG. 8: Propagation of a circular wave. Initial conditions are as in Fig. 6, except that the $\pi/5$ initial phase perturbation is performed on the four central cells of the lattice. Notice that in panel a) the strength of the perturbation ($\pi/5$) is higher than the maximum of the colormap scale.

VI. TUNABLE METAWAVEGUIDES FOR PHASE EXCITATIONS

In the previous sections, we have used periodic boundary conditions for the wavefunction, Eq. (4). Thus we assume that the entire periodic structure is illuminated. This was done for mathematical convenience, in order to introduce and utilize Bloch and Wannier functions, as in condensed matter theory. As far as phase excitations are concerned, the effective ground state defined by the uniform envelope $|\Phi_0|$ of these nonlinear Bloch functions, which extend over the entire domain, acts as an effective optical material for phase waves. Indeed, the effective velocity v —and thus the refractive index— of phase excitations depend on the properties of the underlying nonlinear Bloch function. For different values of power, the nonlinear Bloch function behaves as a different metamaterial —made of light— for the Nambu-Goldstone phase waves propagating on top of it, as unveiled in Fig. 7.

In order to make contact with realistic situations, we need to discuss what happens for finite materials and spatially finite solutions. The expectation, that we will check in this section by numerical computations, is that most of the conclusions can be directly generalized to this case. Notice that, even if the Wannier functions were defined making use of the periodicity conditions, they are essentially localized functions (see Fig. 14 for illustration). Thus, the effective description of Eq. (23) holds essentially unchanged, at least far from the borders of the structure and the predictions about stability and the presence of a Nambu-Goldstone boson excitation apply. Certainly, the larger the finite lattice is, the better the approximation becomes.

Conceptually, since Bloch solutions act as a metamaterial for phase waves, finite size solutions embedded in a photonic lattice can be used as effective waveguides to control phase excitations, as pictorially depicted in Fig. 1. Since at low energies the Poynting vector is approximately given by $\mathbf{S} \sim |\Phi_0|\nabla\alpha$, a full optical control of the electromagnetic flux itself can be also achieved using these metawaveguides.

In Fig. 9, we present some examples of propagation in a finite structure. We define a rectangle of 52×8 unit cells where V takes the form of Eq. (3). Outside the rectangle, we fix $V = V_0$, hindering the diffusion of light to that region. With the method of propagation in imaginary time, we find the stable ground state of the system, which is, approximately, of the form (A1). Then, we introduce, at the border of the rectangle, a perturbation of the phase, similar to the one depicted in Fig. 6 and compute the evolution of the system. As expected, the perturbation of the phase propagates in a similar fashion to the fully periodic case, apart from the fact that, since the perturbation starts from the edge, it moves unidirectionally. For a given g and P/N^2, we can infer the velocity which turns out to coincide, to the few percent level, with that depicted in Fig.7.

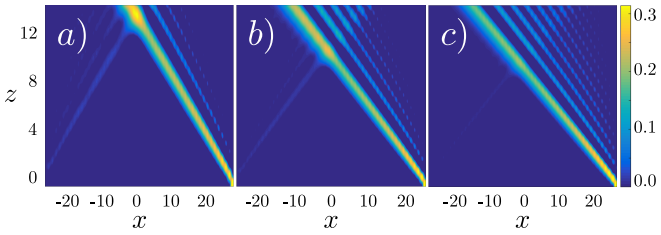

FIG. 9: One-dimensional cuts of the phase perturbation $\phi(x, y = \frac{1}{2}, z)$ moving leftwards, initiated by initial conditions with a $\pi/5$ phase shift in the right-most column. In this example $g = 1$ and $V_0 = 800$. The different panels correspond to different values of P/N^2, namely $P/N^2 = 2$ in panel a), $P/N^2 = 4$ in panel b) and $P/N^2 = 6$ in panel c). The color scale does not cover the full range of the perturbation ϕ, but it has been chosen to optimize the visibility of the plots without missing essential information.

The plots of Fig. 9 show explicitly that velocity of the Nambu-Goldstone phase excitation is different when perturbing solutions with different values of P/N^2, emphasizing the nonlinear character of the dynamics. More

subtly, within each of the plots, small dispersive effects can be appreciated, coming from mild dependences of the velocity on the strength and the wavelength of the perturbation. Curiously, another wave appears moving rightwards from the left border, because the initial condition is not an exact eigenstate. As expected from the discussion of Section V, its velocity is very similar to the one of the main perturbation.

It is interesting to discuss the fate of a perturbation that reaches the boundary of the finite sample. It turns out that the edges act, at least qualitatively, as a reflecting surface. In this way, this structure becomes a paradigmatic case of a metawaveguide —formed by light itself— discussed previously. There are a number of possibilities when considering non-trivial geometries as, e.g., having (3) for some sites and constant $V = V_0$ for the rest. In Fig. 10, we present an example of a U-shaped metawaveguide, and it can be seen how the perturbation turns around due to its interaction with the borders. This opens the possibility of nontrivial manipulation of light through nonlinear effects and of guiding the phase perturbations of Section V. A more detailed analysis of these issues is left for future work.

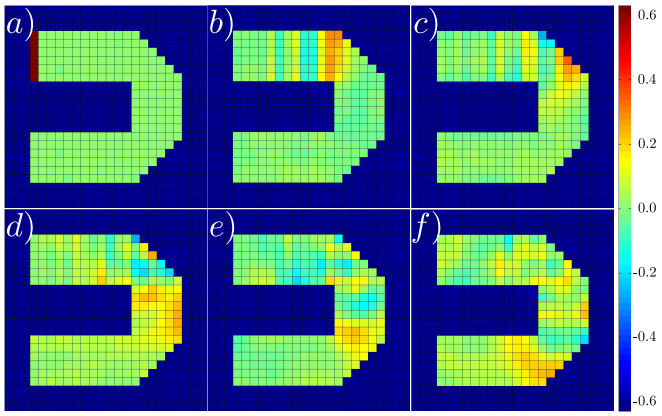

FIG. 10: Bounce of a Nambu-Goldstone phase wave due to reflection in the edge of the structure, resulting in a shift of the propagation direction. The perturbation of the phase is depicted in the lattice sites where Eq. (3) holds. For the rest, where $V = V_0$, the modulus $|\psi|^2$ is nearly vanishing and we just plot them in a uniform color to help visualization. In this example $g = 1$, $V_0 = 800$ and $P/N^2 = 5$. Panels a)-f) correspond, respectively to $z = 0, 4.5, 6, 7.5, 9, 10.5$.

VII. DISCUSSION AND OUTLOOK

An ever-increasing experimental control of the nonlinear propagation of light in nontrivial media has led in recent years to the observation in optical setups of many qualitatively new phenomena. In particular, this has sparked remarkable interest in finding conceptual and quantitative connections with condensed matter physics.

We have shown that methods borrowed from condensed matter physics can be useful for the optical community. We have exploited the nonlinear character of the Schrödinger equation (1) to set the bridge between nonlinear optics and condensed matter in a quantitative manner. Expanding the solutions of Eq. (1) in terms of nonlinear Wannier functions, we have been able to obtain an effective description, Eq. (23), of the dynamics of light propagating within a nonlinear material with a transversally symmetric potential. In this context, we used Landau theory to formally establish the existence of the paradigmatic Mexican hat potential, archetypal of the spontaneous symmetry breaking mechanism appearing in condensed matter and particle physics. This connection has been posed not only qualitatively, but we have computed the effective potential in terms of the coefficients of the problem, showing the key role of the nonlinearity. In light of this effective potential we have been able to determine the stability criteria for the solutions both in the focusing and the defocusing cases.

Two crucial outcomes arise naturally from this point of view: first, the existence of a Nambu-Goldstone boson, which is identified with the phase excitations. We have presented the equation fulfilled by the phase excitation at long distances or, equivalently, at low energies, Eq. (30). Again, this is quantitatively evaluated in terms of the parameters of the problem, agreeing with direct numerical simulations (see Fig. 7, where the predicted and numerically calculated phase velocities are compared). The Nambu-Goldstone boson occurs both for self-defocusing and focusing non-negligible nonlinearity, in the latter case well below the limit for self-focusing and collapse within each lattice cell. The second outcome is the concept of a metawaveguide of light, discussed in Section VI: the phase excitations identified as Nambu-Goldstone bosons can be guided and controlled by the underlying nonlinear localized light structure. We have presented numerical examples of how to guide such a perturbation (cf Fig. 10).

For an experimental observation, and since the main perturbation is in the phase and not in the intensity, detection based on interferometry would be needed, and it could constitute a notable challenge. We have not discussed topological defects like vortices (see e.g. [55] for related work) and domain walls, that are also immediate consequences of the described spontaneous symmetry breaking. Its theoretical and/or experimental analysis is beyond the scope of the present work. Certainly, we have limited the discussion to a particular family of examples. It would be of interest to extend it to more general cases as, e.g., lattices with different symmetries [56], lattices with modulation [57], anisotropic lattices [58] or with the inclusion of gain and loss in parity-time symmetric systems [59].

We have also mentioned that our discussion might be applicable to Bose-Einstein condensates. It is worth mentioning some works that analyze stability in related setups, including one-dimensional [60–63] and two-

dimensional cases [64, 65]. Whether the approach advocated here can provide new insights on these or other similar examples is an open question for the future.

Finally, our work might pave the way for new connections between classical results of condensed matter theory and the propagation of light within properly tuned media. For instance, it could be interesting to devise an optical analogue of the Heisenberg model used in statistical physics to model ferromagnetism. That setup could mimic the subtle structure of phases and phase transitions in two-dimensional systems [66, 67], which is a manifestation of the rich and sometimes counterintuitive dynamics of many body systems. It can also provide a useful framework to analyze the role of light in recent experiments showing superfluidity in polariton condensates [68]. Our work also stresses the role played by phase excitations of nonlinear Bloch modes. Recent experiments indicate the importance of the phase of light over amplitude even in quantum communication systems [69]. Our concept of a metawaveguide of light for the control of phase waves fits nicely within this scenario. These issues are open questions left for future research. Our main claim here is that a *photonic condensed matter* formalism is the perfect theoretical framework to analyze the exciting analogies between condensed matter (and particle physics) and photonic systems.

Appendix A: Bloch and Wannier functions in the linear case

We detail here the linear problem ($P \to 0$ or $g = 0$). Bloch theorem states that the eigenfunctions can be written in terms of Bloch waves $e^{-i\mu_{\mathbf{Q}} z}\varphi_{\mathbf{Q}}(\mathbf{x})$ with

$$\varphi_{\mathbf{Q}}(\mathbf{x}) = \frac{\sqrt{P}}{N} e^{i\mathbf{Q}\cdot\mathbf{x}} u_{\mathbf{Q}}(\mathbf{x}). \tag{A1}$$

There should a band index (the generalization of the quantum number for a single well) but we omit it and restrict ourselves to the lowest band, an approximation that has been kept throughout the paper. Normalization conditions are

$$\int_0^1 dy \int_0^1 dx |u_{\mathbf{Q}}(\mathbf{x})|^2 = 1, \tag{A2}$$

$$\int_\Omega d^2\mathbf{x} \varphi^*_{\mathbf{Q_1}}(\mathbf{x})\varphi_{\mathbf{Q_2}}(\mathbf{x}) = P\,\delta_{\mathbf{Q_1},\mathbf{Q_2}}, \tag{A3}$$

where we have introduced Ω to refer to the whole domain, namely $\int_\Omega d^2\mathbf{x} \equiv \int_{-\frac{N}{2}}^{\frac{N}{2}} dx \int_{-\frac{N}{2}}^{\frac{N}{2}} dy$. The pseudomomentum $\mathbf{Q}$ is discretized because of the finite area and is confined to the first Brillouin cell and, therefore, it can take N^2 values

$$Q_x, Q_y \in \frac{2\pi}{N}\left(-\frac{N}{2}+1, -\frac{N}{2}+2, \ldots, \frac{N}{2}-1, \frac{N}{2}\right), \tag{A4}$$

where we have assumed that N is even. The $u_{\mathbf{Q}}$ is a complex function with period 1, namely $u_{\mathbf{Q}}(x,y) = u_{\mathbf{Q}}(x+1,y) = u_{\mathbf{Q}}(x,y+1)$, which can be computed for a single cell by solving

$$\mu_Q u_{\mathbf{Q}} = -\nabla^2 u_{\mathbf{Q}} + \mathbf{Q}^2 u_{\mathbf{Q}} + V(\mathbf{x}) u_{\mathbf{Q}} - 2i\mathbf{Q}\cdot\nabla u_{\mathbf{Q}}, \tag{A5}$$

with periodic conditions for $u_{\mathbf{Q}}$ at the edges of the unit side cell. We label μ with the pseudomomentum to make explicit its dependence through the dispersion relation. The N^2 Bloch functions form a basis for the states in the lowest band. They can be readily obtained by standard numerical techniques from Eq. (A5). In Figs. 11 and 12, we plot some examples of Bloch waves. In Fig 13 we plot the dispersion relation in the lowest band $\mu(\mathbf{Q})$.

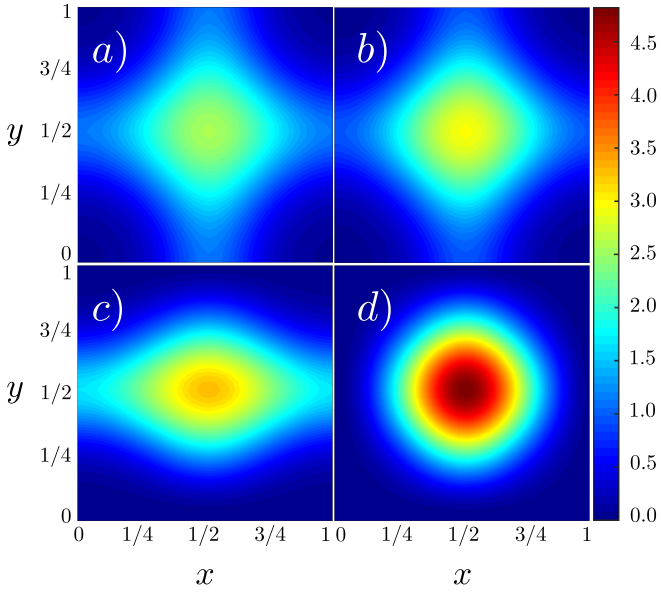

FIG. 11: Representation of $|u_{\mathbf{Q}}(x,y)|^2$ for $V_0 = 100$ and different values of $\mathbf{Q}$. Panel (a): $Q_x = Q_y = 0$. Panel (b): $Q_x = Q_y = \pi/2$. Panel (c) $Q_x = 0$, $Q_y = \pi$. Panel (d): $Q_x = Q_y = \pi$.

Notice that when Q_x and Q_y take values 0 or π, the Bloch functions $\varphi_{\mathbf{Q}}(x,y)$ are real. In particular, $\varphi_{(0,0)}$ is everywhere positive (see panel (a) of Fig. 12) and $\varphi_{(\pi,\pi)}$ changes from positive to negative in alternating cells following a chess board pattern (see panel (d) of Fig. 12). For $Q_x = 0$, $Q_y = \pi$ or viceversa, the phase pattern is striped (panel (c) of Fig. 12). For the rest of $\mathbf{Q}$, the Bloch functions are complex (one could change to a real basis by combining $\varphi_{\mathbf{Q}}$ and $\varphi_{-\mathbf{Q}}$).

Let us now turn to the Wannier functions for the lowest band. They constitute a basis of localized functions and can be written as linear combinations of the Bloch functions,

$$W_{\mathbf{R}}(\mathbf{x}) = \frac{1}{N\sqrt{P}} \sum_{\mathbf{Q}} e^{-i\mathbf{Q}\cdot\mathbf{R}} \varphi_{\mathbf{Q}}(\mathbf{x}), \tag{A6}$$

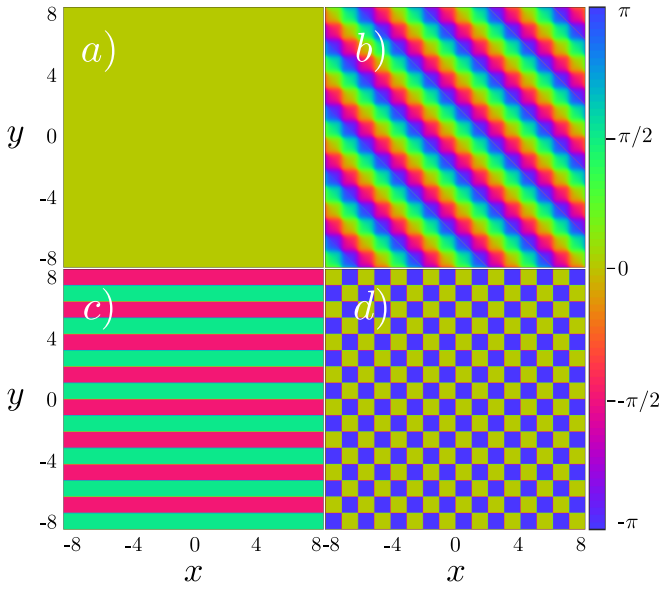

FIG. 12: Representation of the phase of $\varphi_{\mathbf{Q}}(x, y)$ for $V_0 = 100$ and $N = 16$. The four panels show the same four values of $\mathbf{Q}$ considered for Fig. 11.

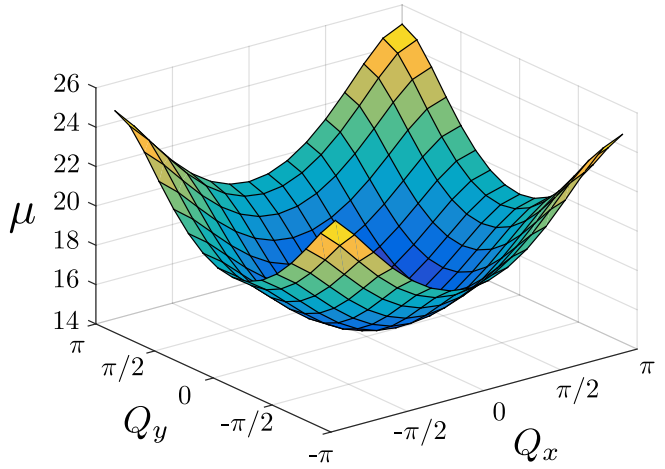

FIG. 13: Dispersion relation $\mu(Q_x, Q_y)$ of the lowest band ($V_0 = 100$).

where the sum runs over the N^2 Bloch momenta and $\mathbf{R}$ takes values corresponding to the center of the N^2 lattice sites

$$R_x, R_y \in \left(\frac{-N+1}{2}, \frac{N+3}{2}, \ldots, \frac{N-3}{2}, \frac{N-1}{2}\right). \quad \text{(A7)}$$

The prefactor is fixed to normalize the $W_{\mathbf{R}}(\mathbf{x})$ as

$$\int_\Omega d^2\mathbf{x} W^*_{\mathbf{R_1}}(\mathbf{x}) W_{\mathbf{R_2}}(\mathbf{x}) = \delta_{\mathbf{R_1},\mathbf{R_2}}. \quad \text{(A8)}$$

Given the Wannier function for one of the sites, all the rest can be found by a spatial translation $W_{\mathbf{R}+\mathbf{n}}(\mathbf{x}+\mathbf{n}) = W_{\mathbf{R}}(\mathbf{x})$, where $\mathbf{n}$ is a lattice vector. In Fig. 14, we represent one of them.

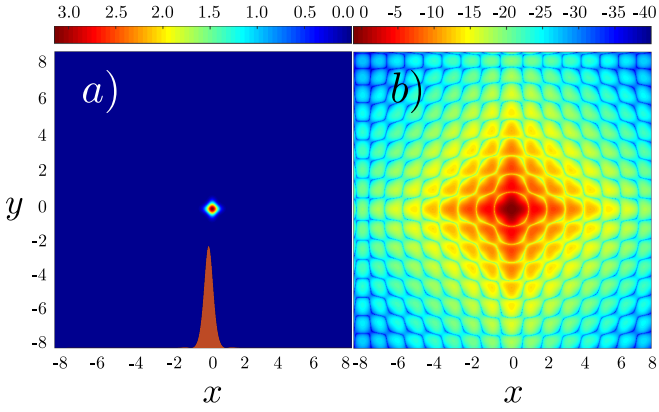

FIG. 14: Square modulus of the Wannier function for $\mathbf{R} = (-\frac{1}{2}, -\frac{1}{2})$, with $V_0 = 100$, $N = 16$. Panel (a) is a colormap for $|W_{\mathbf{R}}(\mathbf{x})|^2$. We also include (in the lower part, in orange) the representation of a one-dimensional section $|W_{\mathbf{R}}(x, -\frac{1}{2})|^2$ (arbitrary units). Panel (b) uses a logarithmic scale, $\ln |W_{\mathbf{R}}|^2$. It shows that $W_{\mathbf{R}}(\mathbf{x})$ has support in the whole domain but becomes negligible far from the cell parameterized by $\mathbf{R}$.

The inverse transformation is

$$\varphi_{\mathbf{Q}}(\mathbf{x}) = \frac{\sqrt{P}}{N} \sum_{\mathbf{R}} e^{i\mathbf{R}\cdot\mathbf{Q}} W_{\mathbf{R}}(\mathbf{x}). \quad \text{(A9)}$$

Appendix B: Definition of the phase perturbation at each lattice site

In sections V and VI we have discussed the propagation of phase perturbations. It is important to introduce an appropriate prescription to represent it. Notice that the phase evolves for the unperturbed solution with propagation constant μ and, moreover, in the staggered case it also changes from cell to cell at any z. Thus, directly plotting the phase is not illustrative. We define here a procedure that is useful to visualize the dynamics (Figs. 5, 7, 8, 9) and also to compute the velocity. Of course, other prescriptions are possible. Our discussion and the physics we have described do not depend on the definition presented here.

First, we assign a phase to each cell by averaging

$$\bar{\phi}_{\mathbf{R}}(z) = \frac{\int d^2\mathbf{x} |\psi|^2 \arg(\psi)}{\int d^2\mathbf{x} |\psi|^2}, \quad \text{(B1)}$$

where the integrals are taken within the lattice site with center at $\mathbf{R}$. This average does not make sense in general because of the cyclic character of the phase, but is well-defined for all the cases at hand, since the in-site phase variations are small, cf. Fig. 4. Then, we subtract the initial phase of the unperturbed solution and

also subtract the phase of a reference cell far from the perturbation.

$$\phi_{\mathbf{R}}(z) = \bar{\phi}_{\mathbf{R}}(z) - \bar{\phi}_{\mathbf{R}}(0) - (\bar{\phi}_{\mathbf{R}_{ref}}(z) - \bar{\phi}_{\mathbf{R}_{ref}}(0)). \quad \text{(B2)}$$

With this prescription, the $\phi_{\mathbf{R}}(z)$ of a stable unperturbed solution is zero for all z. For a perturbed solution, it remains zero far from the perturbation, at least until it reaches $\mathbf{R}_{ref}$.

Acknowledgments

This work is supported by grants FIS2014-58117-P and TEC2014-53727-C2-1-R from Ministerio de Economía y Competitividad (Spain) and grant GPC2015/019 from Xunta de Galicia. MAGM acknowledges support from ERC Advanced Grant OSYRIS, EU IP SIQS, EU PRO QUIC, EU STREP EQuaM (FP7/2007-2013, No. 323714), Fundació Cellex, the Spanish MINECO (SEVERO OCHOA GRANT SEV-2015-0522, FISICATEAMO FIS2016-79508-P), and Generalitat de Catalunya (SGR 874 and CERCA/Program). MAGM and AF acknowledge fruitful discussions with Thomas Busch and Yongping Zhang.

[1] R. Morandotti, U. Peschel, J. Aitchison, H. Eisenberg, and Y. Silberberg, "Experimental observation of linear and nonlinear optical Bloch oscillations," *Physical Review Letters*, vol. 83, no. 23, p. 4756, 1999.

[2] B. Freedman, G. Bartal, M. Segev, R. Lifshitz, D. N. Christodoulides, and J. W. Fleischer, "Wave and defect dynamics in nonlinear photonic quasicrystals," *Nature*, vol. 440, no. 7088, pp. 1166–1169, 2006.

[3] T. Schwartz, G. Bartal, S. Fishman, and M. Segev, "Transport and Anderson localization in disordered two-dimensional photonic lattices," *Nature*, vol. 446, no. 7131, pp. 52–55, 2007.

[4] O. Peleg, G. Bartal, B. Freedman, O. Manela, M. Segev, and D. N. Christodoulides, "Conical diffraction and gap solitons in honeycomb photonic lattices," *Physical review letters*, vol. 98, no. 10, p. 103901, 2007.

[5] D. Leykam, O. Bahat-Treidel, and A. S. Desyatnikov, "Pseudospin and nonlinear conical diffraction in Lieb lattices," *Physical Review A*, vol. 86, no. 3, p. 031805, 2012.

[6] S. Raghu and F. Haldane, "Analogs of quantum-Hall-effect edge states in photonic crystals," *Physical Review A*, vol. 78, no. 3, p. 033834, 2008.

[7] L. Lu, J. D. Joannopoulos, and M. Soljačić, "Topological photonics," *Nature Photonics*, vol. 8, no. 11, pp. 821–829, 2014.

[8] Y. Plotnik, M. A. Bandres, Y. Lumer, M. Rechtsman, and M. Segev, "Topological control of Bloch oscillations of edge modes in photonic lattices," in *CLEO: QELS_Fundamental Science*, pp. FTu2C–4, Optical Society of America, 2015.

[9] F. Maucher, T. Pohl, S. Skupin, and W. Krolikowski, "Self-organization of light in optical media with competing nonlinearities," *Physical review letters*, vol. 116, no. 16, p. 163902, 2016.

[10] Y. V. Kartashov, V. A. Vysloukh, and L. Torner, "Soliton shape and mobility control in optical lattices," *Progress in Optics*, vol. 52, pp. 63–148, 2009.

[11] Y. V. Kartashov, B. A. Malomed, and L. Torner, "Solitons in nonlinear lattices," *Reviews of Modern Physics*, vol. 83, no. 1, p. 247, 2011.

[12] A. Bouk, A. Cucinotta, F. Poli, and S. Selleri, "Dispersion properties of square-lattice photonic crystal fibers," *Optics Express*, vol. 12, no. 5, pp. 941–946, 2004.

[13] J. W. Fleischer, M. Segev, N. K. Efremidis, and D. N. Christodoulides, "Observation of two-dimensional discrete solitons in optically induced nonlinear photonic lattices," *Nature*, vol. 422, no. 6928, pp. 147–150, 2003.

[14] F. Begum, Y. Namihira, T. Kinjo, and S. Kaijage, "Supercontinuum generation in square photonic crystal fiber with nearly zero ultra-flattened chromatic dispersion and fabrication tolerance analysis," *Optics Communications*, vol. 284, no. 4, pp. 965–970, 2011.

[15] Y. Liang, C. Peng, K. Sakai, S. Iwahashi, and S. Noda, "Three-dimensional coupled-wave model for square-lattice photonic crystal lasers with transverse electric polarization: A general approach," *Physical Review B*, vol. 84, no. 19, p. 195119, 2011.

[16] X. Huang, Y. Lai, Z. H. Hang, H. Zheng, and C. Chan, "Dirac cones induced by accidental degeneracy in photonic crystals and zero-refractive-index materials," *Nature materials*, vol. 10, no. 8, pp. 582–586, 2011.

[17] N. W. Ashcroft, N. D. Mermin, and S. Rodriguez, "Solid state physics," 1978.

[18] F. Dalfovo, S. Giorgini, L. P. Pitaevskii, and S. Stringari, "Theory of Bose-Einstein condensation in trapped gases," *Reviews of Modern Physics*, vol. 71, no. 3, p. 463, 1999.

[19] M. Lewenstein, A. Sanpera, V. Ahufinger, B. Damski, A. Sen, and U. Sen, "Ultracold atomic gases in optical lattices: mimicking condensed matter physics and beyond," *Advances in Physics*, vol. 56, no. 2, pp. 243–379, 2007.

[20] N. K. Efremidis, S. Sears, D. N. Christodoulides, J. W. Fleischer, and M. Segev, "Discrete solitons in photorefractive optically induced photonic lattices," *Physical Review E*, vol. 66, no. 4, p. 046602, 2002.

[21] O. Morsch and M. Oberthaler, "Dynamics of Bose-Einstein condensates in optical lattices," *Reviews of modern physics*, vol. 78, no. 1, p. 179, 2006.

[22] L. Santos, M. Baranov, J. I. Cirac, H.-U. Everts, H. Fehrmann, and M. Lewenstein, "Atomic quantum gases in Kagomé lattices," *Physical review letters*, vol. 93, no. 3, p. 030601, 2004.

[23] D. Blömer, A. Szameit, F. Dreisow, T. Schreiber, S. Nolte, and A. Tünnermann, "Nonlinear refractive index of fs-laser-written waveguides in fused silica," *Optics*

Express, vol. 14, no. 6, pp. 2151–2157, 2006.

[24] A. Szameit, J. Burghoff, T. Pertsch, S. Nolte, A. Tünnermann, and F. Lederer, "Two-dimensional soliton in cubic fs laser written waveguide arrays in fused silica," *Optics express*, vol. 14, no. 13, pp. 6055–6062, 2006.

[25] A. Ferrando, M. Zacarés, P. F. de Córdoba, D. Binosi, and J. A. Monsoriu, "Spatial soliton formation in photonic crystal fibers," *Optics Express*, vol. 11, no. 5, pp. 452–459, 2003.

[26] A. Ferrando, M. Zacarés, P. F. de Córdoba, D. Binosi, and J. A. Monsoriu, "Vortex solitons in photonic crystal fibers," *Optics express*, vol. 12, no. 5, pp. 817–822, 2004.

[27] L. Brilland, F. Smektala, G. Renversez, T. Chartier, J. Troles, T. N. Nguyen, N. Traynor, and A. Monteville, "Fabrication of complex structures of holey fibers in chalcogenide glass," *Optics Express*, vol. 14, no. 3, pp. 1280–1285, 2006.

[28] F. Benabid, F. Couny, J. Knight, T. Birks, and P. S. J. Russell, "Compact, stable and efficient all-fibre gas cells using hollow-core photonic crystal fibres," *Nature*, vol. 434, no. 7032, pp. 488–491, 2005.

[29] B. M. Trabold, D. Novoa, A. Abdolvand, and P. S. J. Russell, "Selective excitation of higher order modes in hollow-core PCF via prism-coupling," *Optics letters*, vol. 39, no. 13, pp. 3736–3739, 2014.

[30] Y. S. Kivshar and B. Luther-Davies, "Dark optical solitons: physics and applications," *Physics reports*, vol. 298, no. 2, pp. 81–197, 1998.

[31] G. I. Stegeman and M. Segev, "Optical spatial solitons and their interactions: universality and diversity," *Science*, vol. 286, no. 5444, pp. 1518–1523, 1999.

[32] Á. Paredes, D. Feijoo, and H. Michinel, "Coherent cavitation in the liquid of light," *Physical review letters*, vol. 112, no. 17, p. 173901, 2014.

[33] W. Kohn, "Analytic properties of Bloch waves and Wannier functions," *Physical Review*, vol. 115, no. 4, p. 809, 1959.

[34] Y. Zhang, Z. Liang, and B. Wu, "Gap solitons and bloch waves in nonlinear periodic systems," *Physical Review A*, vol. 80, p. 063815, 2009.

[35] Y. Zhang and B. Wu, "Composition relation between gap solitons and bloch waves in nonlinear periodic systems," *Physical Review Letters*, vol. 102, p. 093905, 2009.

[36] T. J. Alexander, E. A. Ostrovskaya, and Y. S. Kivshar, "Self-trapped nonlinear matter waves in periodic potentials," *Physical Review Letters*, vol. 96, p. 040401, 2006.

[37] L. Carr, C. W. Clark, and W. P. Reinhardt, "Stationary solutions of the one-dimensional nonlinear schrödinger equation. i. case of repulsive nonlinearity," *Physical Review A*, vol. 62, p. 063610, 2000.

[38] L. Carr, C. W. Clark, and W. P. Reinhardt, "Stationary solutions of the one-dimensional nonlinear schrödinger equation. i. case of attractive nonlinearity," *Physical Review A*, vol. 62, p. 063611, 2000.

[39] E. Smirnov, C. Ruter, D. Kip, Y. Kartashov, and L. Torner, "Observation of higher-order solitons in defocusing waveguide arrays," *Optics Letters*, vol. 32, p. 1950, 2007.

[40] S. Coleman, *Aspects of symmetry: selected Erice lectures*. Cambridge University Press, 1988.

[41] P. M. Chaikin and T. C. Lubensky, *Principles of condensed matter physics*. Cambridge university press, 2000.

[42] D. Vollhardt and P. Wi?1/2lfle, *The superfluid phases of helium 3*. Mineola, New York: Dover Publications, Inc., 2013.

[43] S. Coleman, *Aspects of symmetry: selected Erice Lectures*. Cambridge University Press, 1985.

[44] Y. V. Kartashov, V. A. Vysloukh, and L. Torner, "Two-dimensional cnoidal waves in Kerr-type saturable nonlinear media," *Physical Review E*, vol. 68, no. 1, p. 015603, 2003.

[45] T. J. Alexander and Y. S. Kivshar, "Soliton complexes and flat-top nonlinear modes in optical lattices," *Applied Physics B: Lasers and Optics*, vol. 82, no. 2, pp. 203–206, 2006.

[46] M. Petrović, D. Träger, A. Strinić, M. Belić, J. Schröder, and C. Denz, "Solitonic lattices in photorefractive crystals," *Physical Review E*, vol. 68, no. 5, p. 055601, 2003.

[47] D. Neshev, Y. S. Kivshar, H. Martin, and Z. Chen, "Soliton stripes in two-dimensional nonlinear photonic lattices," *Optics letters*, vol. 29, no. 5, pp. 486–488, 2004.

[48] D. Träger, R. Fischer, D. N. Neshev, A. A. Sukhorukov, C. Denz, W. Królikowski, and Y. S. Kivshar, "Nonlinear Bloch modes in two-dimensional photonic lattices," *Optics Express*, vol. 14, no. 5, pp. 1913–1923, 2006.

[49] P. W. Anderson, *Basic notions of condensed matter physics*. Menlo Park, Calif.: Benjamin/Cummings Pub. Co., Advanced Book Program, 1984.

[50] A. Manohar, "Effective field theories," *Perturbative and nonperturbative aspects of quantum field theory*, pp. 311–362, 1997.

[51] P. M. Chaikin and T. C. Lubensky, *Principles of Condensed Matter Physics*. Cambridge University Press, 2000.

[52] M. Greiter, F. Wilczek, and E. Witten, "Hydrodynamic relations in superconductivity," *Mod. Phys. Lett. B*, vol. 03, no. 12, pp. 903–918, 1989.

[53] H. Leutwyler, "Nonrelativistic effective lagrangians," *Phys. Rev. D*, vol. 49, no. 6, pp. 3033–3043, 1994.

[54] M. A. Escobedo and C. Manuel, "Effective field theory and dispersion law of the phonons of a nonrelativistic superfluid," *Phys. Rev. A*, vol. 82, no. 2, p. 023614, 2010.

[55] B. Terhalle, T. Richter, A. S. Desyatnikov, D. N. Neshev, W. Krolikowski, F. Kaiser, C. Denz, and Y. S. Kivshar, "Observation of multivortex solitons in photonic lattices," *Physical review letters*, vol. 101, no. 1, p. 013903, 2008.

[56] A. S. Desyatnikov, N. Sagemerten, R. Fischer, B. Terhalle, D. Träger, D. N. Neshev, A. Dreischuh, C. Denz, W. Krolikowski, and Y. S. Kivshar, "Two-dimensional self-trapped nonlinear photonic lattices," *Optics express*, vol. 14, no. 7, pp. 2851–2863, 2006.

[57] I. L. Garanovich, S. Longhi, A. A. Sukhorukov, and Y. S. Kivshar, "Light propagation and localization in modulated photonic lattices and waveguides," *Physics Reports*, vol. 518, no. 1, pp. 1–79, 2012.

[58] B. Terhalle, A. S. Desyatnikov, C. Bersch, D. Träger, L. Tang, J. Imbrock, Y. S. Kivshar, and C. Denz, "Anisotropic photonic lattices and discrete solitons in photorefractive media," *Applied Physics B: Lasers and Optics*, vol. 86, no. 3, pp. 399–405, 2007.

[59] A. Regensburger, C. Bersch, M.-A. Miri, G. Onishchukov, D. N. Christodoulides, and U. Peschel, "Parity-time synthetic photonic lattices," *Nature*, vol. 488, no. 7410, pp. 167–171, 2012.

[60] C. Menotti, A. Smerzi, and A. Trombettoni, "Superfluid dynamics of a Bose–Einstein condensate in a periodic

potential," *New Journal of Physics*, vol. 5, no. 1, p. 112, 2003.

[61] L. Fallani, L. De Sarlo, J. E. Lye, M. Modugno, R. Saers, C. Fort, and M. Inguscio, "Observation of dynamical instability for a Bose-Einstein condensate in a moving 1D optical lattice," *Physical review letters*, vol. 93, no. 14, p. 140406, 2004.

[62] G. Barontini and M. Modugno, "Dynamical instability and dispersion management of an attractive condensate in an optical lattice," *Physical Review A*, vol. 76, no. 4, p. 041601, 2007.

[63] S.-L. Zhang, Z.-W. Zhou, B. Wu, *et al.*, "Superfluidity and stability of a Bose-Einstein condensate with periodically modulated interatomic interaction," *Physical Review A*, vol. 87, no. 1, p. 013633, 2013.

[64] Z. Chen, B. Wu, *et al.*, "Stability of Bose-Einstein condensates in two-dimensional optical lattices," *Physical Review A*, vol. 81, no. 4, p. 043611, 2010.

[65] Y. Xu, Z. Chen, H. Xiong, W. V. Liu, B. Wu, *et al.*, "Stability of p-orbital Bose-Einstein condensates in optical checkerboard and square lattices," *Physical Review A*, vol. 87, no. 1, p. 013635, 2013.

[66] N. D. Mermin and H. Wagner, "Absence of ferromagnetism or antiferromagnetism in one-or two-dimensional isotropic Heisenberg models," *Physical Review Letters*, vol. 17, no. 22, p. 1133, 1966.

[67] J. M. Kosterlitz and D. J. Thouless, "Ordering, metastability and phase transitions in two-dimensional systems," *Journal of Physics C: Solid State Physics*, vol. 6, no. 7, p. 1181, 1973.

[68] G. Lerario, A. Fieramosca, F. Barachati, D. Ballarini, K. S. Daskalakis, L. Dominici, M. De Giorgi, S. A. Maier, G. Gigli, S. Kéna-Cohen, and D. Sanvitto, "Room-temperature superfluidity in a polariton condensate," *Nat Phys*, p. 2228, 2017.

[69] Y. Cao, Y.-H. Li, Z. Cao, J. Yin, Y.-A. Chen, H.-L. Yin, T.-Y. Chen, X. Ma, C.-Z. Peng, and J.-W. Pan, "Direct counterfactual communication via quantum zeno effect," *Proc Natl Acad Sci USA*, vol. 114, no. 19, pp. 4920–4924, 2017.